REPORT DOCUMENTATION PAGE

Form Approved
OMB No. 0704-0188

1. AGENCY USE ONLY (Leave blank)	2. REPORT DATE	3. REPORT TYPE AND DATES COVERED
	March 18, 1998	Technical Report 6/01/97 - 5/31/98

4. TITLE AND SUBTITLE
Synthesis and Characterization of Polypyrrole/Vanadium Pentoxide Nanocomposite Aerogels

5. FUNDING NUMBERS
N00014-93-1-0245
R&T Code: 4133041
PR Number: 98PRO-3338

6. AUTHOR(S)
H.P. Wong, B.C. Dave, F. Leroux, J. Harreld, B. Dunn and L.F. Nazar

7. PERFORMING ORGANIZATION NAME(S) AND ADDRESS(ES)
Bruce S. Dunn
Department of Materials Science and Engineering
University of California
Los Angeles, CA 90095-1595

8. PERFORMING ORGANIZATION REPORT NUMBER
Technical Report No. 11

9. SPONSORING/MONITORING AGENCY NAME(S) AND ADDRESS(ES)
Office of Naval Research
Chemistry Division
800 North Quincy Street
Arlington, VA 22217-5660

10. SPONSORING/MONITORING AGENCY REPORT NUMBER

11. SUPPLEMENTARY NOTES
To be published in Journal of Materials Chemistry

12a. DISTRIBUTION/AVAILABILITY STATEMENT
Reproduction in whole or in part is permitted for any purpose of the United States Government. This document has been approved for public release and sale; its distribution is unlimied.

12b. DISTRIBUTION CODE

13. ABSTRACT (Maximum 200 words)

Vanadium pentoxide/polypyrrole aerogel (ARG) composites were synthesized by sol-gel routes, and investigated as cathode materials in Li batteries. The primary method utilized simultaneous polymerization of pyrrole and vanadium alkoxide precursors. Supercritical drying yielded high surface (150-257 m^2/g) aerogels with densities between 0.1 and 0.2 g/cc. The interaction between the polypyrrole (PPy) and V_2O_5 aerogel in the nanocomposites was probed using IR spectroscopy. Our results suggest that the inorganic and organic components strongly interact, thus impeding the vanadium condensation process. Hence, the PPy/V_2O_5 nanocomposites exhibited lower electrical conductivity with increased polypyrrole content. The deleterious effect of the conductive polymer on the bulk conductivity does not necessarily affect the electrochemical properties of these materials. Nanocomposite materials that were subjected to post-oxidative treatment show enhanced Li insertion capacity compared to the pristine ARG. The physical properties of these "nanocomposite aerogels" are different from "microcomposites" prepared by an alternate route, in which the oxide gel is formed in the presence of a dispersion of preformed micron-sized polypyrrole particles.

14. SUBJECT TERMS
Organic-inorganic aerogels, vanadium oxide, polypyrrole, lithium insertion

15. NUMBER OF PAGES

16. PRICE CODE

17. SECURITY CLASSIFICATION OF REPORT	18. SECURITY CLASSIFICATION OF THIS PAGE	19. SECURITY CLASSIFICATION OF ABSTRACT	20. LIMITATION OF ABSTRACT
Unclassified	Unclassified	Unclassified	

OFFICE OF NAVAL RESEARCH

GRANT: N00014-93-1-0245
R&T Code: 4133041
PR Number: 98PRO-3338

Dr. Richard Carlin

Technical Report #11

Synthesis and Characterization of Polypyrrole/Vanadium Pentoxide Nanocomposite Aerogels

by

H.P. Wong, B.C. Dave, F. Leroux*, J. Harreld, B. Dunn and L.F. Nazar*

Prepared for publication

in

Journal of Materials Chemistry

Department of Materials Science and Engineering
University of California, Los Angeles
Los Angeles, CA 90095-1595

*Department of Chemistry
University of Waterloo
Waterloo, Ontario, Canada N2L 3G1

March 18, 1998

Synthesis and Characterization of Polypyrrole/Vanadium Pentoxide Nanocomposite Aerogels

H.P. Wong[a], B.C. Dave[b], * F. Leroux[c], J. Harreld[a], B. Dunn[a] and L.F. Nazar[c*]

[a] *Department of Materials Science and Engineering*
University of California, Los Angeles
Los Angeles, CA 90095-1595

[b] *Department of Chemistry and Biochemistry*
Southern University of Illinois at Carbondale
Cqrbondale, Illinois

[c] *Department of Chemistry*
University of Waterloo, Canada
Waterloo, Ontario, Canada N2L 3G1

Abstract

Vanadium pentoxide/polypyrrole aerogel (ARG) composites were synthesized by sol-gel routes, and investigated as cathode materials in Li batteries. The primary method utilized simultaneous polymerisation of pyrrole and vanadium alkoxide precursors. Hydrolysis of $VO(OC_3H_7)_3$ using pyrrole/water/acetone mixtures yielded monolithic green-black gels with polypyrrole/V ratios ranging from 0.15 to 1.0. Supercritical drying yielded high surface (150-257 m^2/g) aerogels with densities between 0.1 and 0.2 g/cc, that were of sufficient mechanical integrity to allow them to be cut without fracturing. TEM studies of the ARGs show that they are comprised of fibers similar to that of V_2O_5 ARG's, but with a significantly shorter chain length. The interaction between the polypyrrole (PPy) and V_2O_5 aerogel in the nanocomposites was probed using IR spectroscopy. Our results suggest that the inorganic and organic components strongly interact during the initial stages, thus perhaps impeding the vanadium condensation process. Hence, the PPy/V_2O_5 nanocomposites exhibited lower electrical conductivity with increased polypyrrole content. The addition of $(NH_4)_2S_2O_8$ as an oxidizing agent improved the conductivity of the nanocomposites. The deleterious effect of the conductive polymer on the bulk conductivity does not necessarily affect the electrochemical properties of these materials. Nanocomposite materials that were subjected to post-oxidative treatment show enhanced Li insertion capacity compared to the pristine ARG. The physical properties of these "nanocomposite aerogels" are different from "microcomposites" prepared by an alternate route, in which the oxide gel is formed in the presence of a dispersion of preformed micron-sized polypyrrole particles.

Introduction

Supercritical drying of monolithic V_2O_5 gels formed from the rapid hydrolysis of vanadium alkoxides yield aerogels (ARGs) that display extremely high surface areas and controllable porosity.[1] These characteristics make them attractive as cathodes in rechargeable lithium batteries where kinetic barriers due to Li access and transport within the crystalline lattice can pose limits to attaining theoretical capacities.[2] Their low electrical conductivity can be minimized by the use of extremely thin films supported on a conductive substrate, or partially overcome by the incorporation of conductive carbon additives. Li batteries comprising electrodes of these materials demonstrate relatively high lithium insertion capacity and energy density.[3] Nevertheless, neither of these methods fully capitalize on the high surface area available in the materials. An potential alternative to the addition of carbon is the incorporation of a conducting polymer into the ARG structure. Polypyrrole (PPy) is an electronically conductive polymer which has received considerable attention due to its high electrical conductivity and stability in electrochemical environments. PPy also has been shown to be a promising cathode in lithium secondary cells,[4] although maintainance of surface area and hence access of ions to the polymer structure remains a difficulty in this pseudo-capacitive type material.[5] The support of PPy on high surface area V_2O_5 aerogels thus offers the prospect of maximizing the performance of both inorganic and organic components.

Fabrication of these materials in monolithic form presents some challenges. The synthesis of low surface area *xerogel* V_2O_5-polymer nanocomposite crystallites is well established. Amongst the most interesting materials are those of polyaniline[6] and polypyrrole[7] in which the polymer chains have been interleaved between the V_2O_5 sheets by an *in-situ* intercalation and oxididative polymerisation method. At high polymer content, these materials show improved conductivity compared to pristine V_2O_5 xerogels. Our recent electrochemical studies on these nanocomposites,[8] in addition to similar studies of polyaniline nanocomposites of $HTaWO_6$[9] and MoO_3, have all shown enhancement in lithium ion mobility on incorporation of the polymer.[10] These findings have prompted us to develop methods for the synthesis of ARG - based polymer/oxide composites.

Our strategy described here involves *in-situ* polymerisation of the pyrrole monomer during the sol-gel condensation process. A preliminary account of this work has been reported.[11] The oxidative

coupling of the pyrrole units (by the vanadium oxide) to form PPy, is simultaneous with polymerisation of the inorganic oxide which is catalysed by reaction with the pyrrole. The result is in a monolithic inorganic/organic hybrid gel in which both components are mixed at the nanocomposite level. For comparison, we have also investigated *in-situ* encapsulation of preformed colloidal particles of PPy within the V_2O_5 gel, during the initial stages of the sol-gel condensation process. This method yields a monolithic homogeneous "micro"composite of the V_2O_5 and PPy. Our investigation probes the interaction of the inorganic and organic components of these ARGs, its effect on the electrical properties, and on electrochemical Li insertion into the nanocomposite ARG.

Experimental

Synthesis and Physical Properties

Vanadium pentoxide ARGs containing polypyrrole were synthesized using two variations of the sol-gel method. Both methods are based on our prior work involving the hydrolysis and condensation of vanadium isopropoxide (Gelest) in acetone/water solutions.[1] In the first method (simultaneous polymerisation), the alkoxide and pyrrole (Aldrich) were mixed, and a vial containing the mixture was placed in an ice bath along with a vial containing the water/acetone mixture. A typical composition was 1.0 $VO(OC_3H_7)_3$: 40 H_2O: 17 $(CH_3)_2CO$: y C_4H_4NH. The two vials were allowed to cool prior to mixing, after which the water/acetone mixture was stirred into the vial containing the alkoxide and pyrrole. Samples without pyrrole were also prepared. The sol was stirred and cast into rod-shaped glass vials. Gelation occured within 75 seconds without pyrrole to yield transparent dark red gels; the pyrrole containing materials gelled within 10-30 seconds resulting in deep green opaque gels. The ratio of pyrrole (P) was varied from 0.15 to 1.0 moles /$VO(OR)_3$, and the water-acetone molar ratio was also varied extensively over a wide composition range to obtain compositions $PPy_{2P}V_2O_5$ which resulted in ARGs with sufficient mechanical integrity to allow the monolithic samples to be cut into discs with a diamond saw for measurements of bulk electrical conductivity. Some preparations also involved the pre-oxidation of the pyrrole monomer with $(NH_4)_2S_2O_8$ (0.075 mole/V) prior to its reaction with the alkoxide.

V_2O_5/polypyrrole microcomposite ARGs were synthesized by forming the oxide gel in the presence of a dispersion of the preformed PPy. This approach is in contrast to others reported in which pyrrole is polymerized *in situ* around dispersed particles of oxide[12] or carbon black.[13] Pyrrole was polymerized in a 2.5 M solution of ferric chloride in diethyl ether (4:1 moles, $FeCl_3$:Py) according to the procedure used by Myers.[14] The precipitated PPy was vacuum dried for 4 h at 65 °C and ground into a fine powder. The conductivity of the polymer thus prepared was 54 S/cm, as determined by two-point AC conductivity measurements on pressed pellets (see below). The desired quantity of polymer was then added to a solution of water and acetone. A relatively stable dispersion was formed by mixing the solution using an automatic stirrer at 8000 rpm. Vanadyl triisopropoxide and the polymer dispersion were chilled to 0 °C in separate containers. The polymer dispersion was poured into the casting vial containing the vanadyl alkoxide (1:40:18 moles, V:H_2O:acetone), shaken quickly and allowed to gel. Gelation occurred within 10 s. The resulting composite gels were treated as described above.

The wet gels were aged for 4 days in their sealed containers with a 1mm hole in the cap, to allow for slow evaporation of the solvent within the wet gel. This resulted in a small amount of shrinkage (15%) and densification that strengthened the gels. After aging, the gels were removed, and immersed in acetone for a day to promote exchange of the water in the gel pores for acetone. This procedure was repeated 4 times to ensure complete exchange. The gels were transferred to the pressure vessel (Polaron E3000 Critical Point Dryer) for supercritical extraction by CO_2.[1] The resultant dark-green cyclinder-shaped monoliths had dimensions of approximately 1 cm in diameter, and 3 cm in length.

The density of the aerogels was determined using a pycnometer vial filled with Hg. Surface area measurements (N_2 absorption) were conducted on a Micromeritics Flowsorb 2300 system and analyzed by the BET method. The nanocomposites powders were vacuum dried at 125°C for 3 hours prior to degassing the samples. TGA (Dupont 9900 Thermal Analysis System) measurements were used to determine molar composition of the pyrrole/V_2O_5 gels. Analysis of the materials was performed in N_2 and air using a heating rate of 10°C/min to 600°C. TEM was performed on a Phillips CM30. Samples were prepared by dipping holey carbon grids into a sonicated dispersion of the ARG fragments in hexane. FTIR data were obtained as KBr pellets on a Nicolet FT-IR spectrometer operating between 400 cm^{-1} to 4,000 cm^{-1}. Samples of V_2O_5 and $PPy_{2P}V_2O_5$ ARGs were prepared for detailed FTIR spectroscopy,

using ^{18}O-labeled water and deuterium-labeled water (D_2O). X-ray powder diffraction (XRD) patterns of the crushed ARGs were obtained on a Siemens D500 X-ray diffractometer equipped with a diffracted beam monochromator, using Cu-Kα radiation. Samples were scanned at a step scan rate of 0.02 degrees/second.

Electrical and electrochemical measurements

Aerogel discs were used to measure electrical conductivity. The discs were coated with gold at both ends using a plasma sputtering system (Anatech, Ltd. Hummer VI-A). Two-point AC complex impedance measurements (20 Hz to 1 MHz) were performed using a computer-controlled Hewlett Packard 4284A Precision LCR meter using a 0.1 Vrms test signal, and ensuring ohmic contact. The discs were heated at 150°C for 24 hours prior to taking measurements. Variable temperature conductivity measurements were made in the range from 180°C to 25°C in flowing argon (99.995%).

To study Li insertion in the materials, composite electrodes were prepared from active material, carbon black (Super S, Alpha Chemicals) and Kynar Flex 2820-00 as the organic binder. The powders in the weight proportion 80, 15, 5, respectively, were mixed in cyclopentanone and the slurry was spread onto an aluminium disk. Before assembling the cells in the glove box, the composite electrodes were heated at 80°C for 3 hours in order to remove the free water without altering the morphology of the ARGs. A solution of 1.0M $LiClO_4$ in propylene carbonate (PC, Aldrich) was used as the electrolyte. The PC was twice distilled under vacuum from activated molecular sieves through a glass-bead filled column prior to its use.. Swagelock type cells were assembled in an argon filled glove box containing less than 2ppm of water and oxygen. Electrodes had a surface area of 1.0 cm^2 and contained ~ 2mg of active material.

A multichannel galvanostatic/potentiostatic system (MacPile™) was used for the electrochemical study. Voltage was applied in steps of 10mV/0.2h and 10mV/0.02h; alternatively, in the galvanostatic mode, the voltage dependance *vs* Li composition for the composite electrode was studied under varying current densities. The most common corresponded to an intercalation of 1 Li in 20 hours.

The electronic density (per mole V^{-1}) *vs* voltage was calculated by numerical differentiation of the voltage composition dependance curves. The charge cycle is denoted by positive values. For low current densities, the dx/dV*vs* V curves gives identical information to a cyclic voltamogramm, in terms of position of Li potential sites and their relative occupancies.

Results

Synthesis

Figure 1 is a composition map for the polypyrrole/V_2O_5 nanocomposites with a fixed pyrrole ratio of 0.15 (corresponding to a composition $PPy_{0.3}V_2O_5$). Water and acetone ratios were varied over a wide range which enabled us to obtain monolithic, homogeneous gels with good mechanical integrity. Optimum properties were found in the range corresponding to samples 5 to 9. Higher water ratios and lower acetone ratios produced more robust gels, but increased the gelation rate. Increased pyrrole concentration decreased the strength of the gels, although this could be compensated by a higher water ratio and lower acetone ratio. Improved integrity was also achieved by partially drying the wet gel during the aging treatment under ambient conditions prior to supercritical drying. This resulted in slight densification of the ARGs compared to those which were not subjected to this treatment. For pure V_2O_5 ARGs, the partial drying treatment produces samples with densities in the range of 0.2 g /cc, as compared to 0.1 g/cc obtained without the treatment. The addition of pyrrole has little effect on ARG density, as the [PPy]V_2O_5 ARGs (all partially dried) exhibited slightly increased densities of about 0.2 g/cc (**Table 1**).

We also undertook other synthetic strategies to prepare these nanocomposites, in an effort to examine the effect of inorganic/organic interaction. The second approach involved the addition of an aqueous dispersion of pre-polymerized polypyrrole to the vanadium alkoxide thus triggering hydrolysis of the alkoxide. Hydrolysis was sufficiently rapid (within 10s) that the polymer particles were encapsulated in the V_2O_5 gel network.

Physical Properties

BET analysis indicated that the surface area of the nanocomposites prepared by simultaneous polymerisation are similar to that measured for pure V_2O_5 ARGs. The $PPy_{2P}V_2O_5$ samples exhibited

surface areas between 150 and 250 m^2/g (**Table 1**). The surface area of these pure V_2O_5 ARGs is lower than that found previously (300-400 m^2/g) for samples synthesized under different precursor ratios.[1] Samples prepared by the dispersion method exhibited a slightly lower surface area of 80-140 m^2/g due to the presence of micron-sized PPy particles within the oxide matrix (*vide infra*).

Pure vanadium pentoxide ARGs are hydrated oxides of the composition $V_2O_5 \cdot nH_2O$ with $n = 2.0$ to 2.2. At approximately 150°C, the water layer between the fibers is no longer continuous and the conductivity of $V_2O_5 \cdot nH_2O$ becomes essentially electronic. **Figure 2** shows a TGA curve for the $PPy_{0.5}V_2O_5$ nanocomposite, in which two characteristic weight losses are observed. The initial step below 125°C is due to loosely bound water in the material. The remaining feature at 250°C is attributed to a combined loss of water and PPy. This behavior is very similar to that reported for PPy/V_2O_5 xerogels, for which PPy decomposition also occurs above 250°C.[7] Assuming that all of the PPy is combusted by 400°C, there are still approximately 1.2 moles of water remaining in the nanocomposites at 180°C. The composition of the as-prepared ARG nanocomposites can be calculated as $PPy_{2P}V_2O_5 \cdot nH_20$, where P = 0.15-1.0 and n = 2.4 - 3.1.

XRD studies showed that both V_2O_5 and $[PPy]V_2O_5$ ARG's exhibit a very low degree of crystallinity compared to the respective xerogel forms. The relatively amorphous structure resulted in a very broad, weak reflection corresponding to an interlayer spacing of about 12.5Å, similar to that reported previously for pure V_2O_5 ARGs. Additional poorly resolved reflections in the region 2θ = 6-9º were observed, in the same region reported for PPy intercalated in V_2O_5 xerogel galleries.[7] This results are suggestive of some intercalation of PPy in the ARG, albeit in a highly disorganized structure that is not amenable to X-ray study.

The poorly organized nature of the ARG nanocomposites was also very evident in the TEM micrographs. Whereas the fibers for the V_2O_5 ARG displayed a long, ribbon-like structure similar to that previously reported for vanadate xerogels (**Figure 3a**),[1] those of the polymer-ARG were much shorter in length, and were aggregated in a random fashion (**Figure 3b**). This morphology is substantially different than the ARG nanocomposites prepared using the dispersion method, which consisted of PPy particles encapsulated in the fibrous V_2O_5 network, as shown by SEM (**Figure 3c**). Thus, the

simultaneous copolymerisation method produces a nanocomposite that is characterized by almost molecular level mixing which appears to inhibit growth of the inorganic network. Conversely, the dispersion method produces what might be classified as a microcomposite.

FTIR Analysis.

The FTIR spectrum of the ARG nanocomposite between 2000 and 400 cm^{-1} (not shown) displays strong bands in the 1600-900 cm^{-1} region that are diagnostic of PPy, and their position and intensities show that the conductive form of the polymer is produced. The chain length and conductivity of the PPy can be estimated from the ratio of the A'/B' bands at 1580 and 1460 cm^{-1} respectively. Studies of bulk PPy show a linear relationship between this ratio and the log of the conductivity of the polymer.[15] Using this data, together with the A'/B' value in the nanocomposite,

($\cong$ 5.0), interpolation indicates that the PPy component appears to be relatively conductive (1 S/cm). The bands also exhibit slight shifts from those of bulk, p-doped PPy, suggesting that a substantial interaction with the V_2O_5 framework occurs. More insight on the nature of this interaction is provided by examining the changes occurring in the vibrational modes of the inorganic lattice which dominate the spectrum.

Due to the presence of V-O-V units, two vibrational modes, the symmetric stretch (ν_{sym}) and the asymmetric stretch (ν_{as}) are expected to occur in the vibrational spectrum in the 400-800 cm^{-1} range.[16] O^{18} isotope shifts of samples prepared using O^{18}-labeled water were used to identify these modes. The band 542 cm^{-1} in the natural abundance sample (figure not shown) downshifts to 521 cm^{-1} in the O^{18}-labeled samples. As the symmetric stretch of the M-O-M containing structures usually occur in this region, this mode is assigned as ν_{sym}. A low intensity peak at 772 cm^{-1} is also found to shift upon O^{18} substitution and is tentatively assigned as ν_{as}.

The assignment of these modes was used to characterize the structural changes associated with PPy incorporation. We found that both modes shift to higher wavenumber with increasing PPy content, with a direct correlation of upshift to PPy content (**Table 1**). The ν_{sym} mode at 542 cm^{-1} in the pristine

V_2O_5 sol-gel is increased to 580 cm^{-1} in samples of $PPy_{1.0}V_2O_5$ (**Figure 4**). The data suggests a highly interacting V_2O_5-PPy host-guest system in which the coordination environment at the metal centers is affected by interaction with the organic component. Prior studies on V_2O_5 reported by Savariault *et.al* with pyridine as an intercalant resulted in lowered frequencies of the V_2O_5 modes in the 500-800 cm^{-1} region.[17] The downshifts were ascribed to coordination of pyridine to vanadium ions which leads to weakening of the V-O-V bonds. Similar downshifts have also been observed with anilinium ion as a dopant.[18] Our data shows that intercalation of PPy induces a different mode of interaction with the V_2O_5 matrix leading to a different structural perturbation of the matrix.

In contrast, the vanadyl stretch ($\nu_{V=O}$) which occurs at 1000 cm^{-1} in the V_2O_5 ARG, shifts down to 993 cm^{-1} on incorporation of the polymer, implying either increased V^{4+} content in the lattice or a weakening of the V=O bond. Similar downshifts have been previously observed with pyridine and anilinium ions as intercalates in V_2O_5, and our results are in general agreement with vibrational data obtained with other N-containing species as intercalation guests (**Table 2**). In these cases the shifts are a result of reduced V-O-V bond length caused by weak binding of the nitrogen atom of the pyrrole ring to the sixth apical coordination site on the square-pyramidal V site.

For the PPy/V_2O_5 nanocomposites, the major factor in the shift of the V=O band, however, is the contribution of H-bonding interactions. In order to determine the nature of the H-bonding interaction between the PPy polymer and the inorganic matrix, spectra were obtained on samples prepared in D_2O. FTIR spectra of pure V_2O_5 materials show an absence of isotope shifts for the ν(V=O) mode at 1000 cm^{-1}, indicating a lack of hydrogen bonding interactions. This mode in $[PPy]_{1.0}V_2O_5$ ARG's, however, show sensitivity to deuterium substitution. The V=O mode at 993 cm^{-1} downshifts to 987 cm^{-1} in the D_2O-labeled samples (**Figure 5**). The development of H-bonding interactions between the V_2O_5 matrix and the polymer appears to be a principal factor for decreased V=O bond strength in the nanocomposite materials. Collectively, our results therefore suggest a presence of V=O···H type units in the nanocomposite materials. Significantly, both the shifts in the V-O-V bands, and the V=O bands were not observed in the microcomposite materials prepared by the dispersion method.

Electrical Properties

The nanocomposite samples were heat treated at 180°C prior to complex impedance measurements. TGA analysis showed that the nanocomposites lose 10% of their weight by this temperature, corresponding to a composition of $[PPy]_{2P}V_2O_5 \cdot 1.2H_2O$. The dispersion observed in the complex impedance plane indicates that there is an ionic contribution to the conductivity for samples with pyrrole ratios greater than P = 0.7. At lower pyrrole contents, and in pure V_2O_5, only electronic conduction is observed. Moreover, the PPy/V_2O_5 microcomposites prepared by the dispersion method also exhibited only electronic conduction.

Figure 6 shows the results of the complex impedance analysis for both the nanocomposites and microcomposites. For the $PPy_{2P}V_2O_5$ nanocomposites (**Figure 6a**), the conductivity *decreases* with increasing PPy content. At 25°C, the conductivity decreases by a factor of 10^4 as P increases from 0 to 0.9 (Table 1). The activation energy changes only slightly from that of pure V_2O_5 (0.23 eV to 0.32eV). In contrast to this behavior, the microcomposites exhibit no change in conductivity from that of pure V_2O_5 despite the fact they contain as much as 75 mole% PPy (**Figure 6b**).

Electrochemical Lithium Insertion in Nanocomposite Aerogels

V_2O_5 Aerogel

In order to understand the effect of the PPy incorporation into the ARG, V_2O_5-ARG was first studied as an electrode material in a Li battery as a function of discharge depth, and cycling rate. The first discharge cycle is shown in **Figure 7a** down to 1.8V. Two Li potential sites are evident at 2.9 and 2.5V vs Li. Both sites are normally present in the V_2O_5 xerogel. The corresponding mirror image of these redox peaks is observed in charge.

The second and third cycles were then recorded on decreasing the discharge cut-off voltage to 1.2V *vs* Li. An additional reduction process appears at 1.5V, which modifies the subsequent charge process. By contrast to the first oxidation sweep, three defined oxidation peaks are now observed during the following charge (1.65, 2.15 and 2.65V). This transformation continues in the following cycle in this 1.2-3.8 window. On discharge, small shifts occur in the position of the reduction peaks. In charge,

however, the lower potential Li site disappears, and a well-defined site further develops at 2.15V. Greater Li occupancy is also observed at high voltage, marked by the presence of a large shoulder on the charge curve. Hence, we have found that these electrochemical processes are very sensitive to the reduction depth. The redox processes that we observe during the intercalation-deintercalation of Li are different from those reported by Smyrl *et. al.*. They do not observe the 2.5V Li site either in discharge or in charge, as they did not cycle below 1.8V.[3b,c]

Kinetic factors also play a role in the site occupancies. We have used cyclic voltammetry to examine the effect of rate on the relative site occupancies. For average to high cycling rates (10mV/0.2h to 10mV/0.02h), the ratio of the occupancies of the 2.5 and 2.9V Li site in discharge is reversed (**Figure 7b**); nevertheless, the 2.5V site is still present. The anodic peak at 2.15V is particularly sensitive to the cycling rate, as it is not observed at the higher rate.

At the same cycling rate, the V_2O_5-ARG performs better than the xerogel, as previously reported. Even though the theoretical capacity is lower for the aerogel than for the xerogel (due to a greater contribution of V^{4+}), the experimental Li capacity is a factor 1.7 times greater (1.105 and 1.80F/mol for V_2O_5-XRG and ARG, respectively). This outlines the importance of the kinetic factors, and shows that there is excellent accessibility of Li sites in this high surface area material. Furthermore, the V_2O_5-ARG displays good stability in the 1.2-4.0V window, giving a specific capacity of 400mAh/g under these conditions.

Effect of PPy content on the electrochemical response.

The dependence of the voltage *vs* first discharge capacity as a function of the polymer content is shown on **Figure 8**. The effect of the PPy on the electrochemical response is to clearly *decrease* the Li capacity, in accordance with the electrical measurements which showed decreased conductivity as a function of polymer content. In the electrochemical sense, this can be explained by a lowering of the oxidation potential of the vanadium oxide component (*via* increased formation of V^{4+}) as a result of *in-situ* reaction with the pyrrole monomer (*vide infra*).

The modification of the Li sites on polymer incorporation is illustrated in **Figure 9**. The nanocomposites display two distinct processes in discharge, shifted to some degree from their respective

positions in V_2O_5. $[PPy]_{0.3}V_2O_5$ is different from the other compositions, in that Li occupies the 2.5 and 2.9V Li sites as in V_2O_5, in addition to two new sites at 2.1 and 2.25V. Li insertion in the nanocomposites gives rise to broader reduction peaks, and hence the sites are less well ordered than in V_2O_5. The same factor has been observed for xerogel-derived [PPy] V_2O_5, in which incorporation of the polymer results in a wider distribution of the Li site potential.[8b,c]

Effect of an oxidation treatment.

We attempted to offset the lower capacity of the nanocomposite ARGs by reoxidizing the material. Two different oxidation treatments were carried out; *in-situ* and post-oxidation. The effect of these treatments on the $[PPy]_{0.3}V_2O_5$ electrochemical response is displayed in **Figure 10.** The *in-situ* method in which the oxidizing agent (peroxydisulfate) is involved during the formation of the nanocomposite, had a negative effect on the electrochemical response. The *in-situ* oxidized materials give rise to a lowered Li capacity of less than 1F/mole, suggesting that though the vanadium is in a higher oxidation state in this case, the Li ions do not have access to the redox centers.

On the other hand, after post-oxidative treatment under oxygen, the capacity of the nanocomposite is significantly improved (curve 4, **Figure 10**), yielding a fully reversible capacity of 2.2F/mol. Step potential electrochemical spectroscopy (SPES) experiments have shown that a better occupancy of the 2.5V Li site is mostly responsible for the enhanced capacity of the O_2 treated material. Moreover, this material is capable of rapid Li ion diffusion at high cycling rates. These results will be described more fully in a subsequent publication.

Discussion

Nature of the V_2O_5-PPy Interaction. The TEM, conductivity and FTIR results collectively point to an intimate and strong interplay of the inorganic and organic components in the nanocomposite material, as opposed to the microcomposite material. There are two types of vibrational modes whose shifts indicate the nature of the interaction. The shifts of the ν(V=O) modes indicate that increased H-bonding effects are observed in the nanocomposite material. The H-bonding upon PPy incorporation can be ascribed to

interaction with the organic moiety. The -NH functional group in the PPy is an excellent candidate for an H-bonding interaction. Acid-base type reactions between a basic dopant and the V_2O_5 framework have been previously proposed as the dominant mode of interaction.[19] The strong H-bonding interactions between the -NH group of PPy and the V=O moiety represent a limiting example of such interactions. We propose a tentative model of the interactions that may be operative in the nanocomposite materials in **Figure 11.**

The second type of vibrational mode that is affected by the interaction is the V-O-V stretch. Prior studies on intercalation of N-containing species indicate that the V-O-V modes are downshifted upon introduction of the guest species. The observed upshifts of both the vibrational modes, ν_{sym}(V-O-V) and ν_{as}(V-O-V), on PPy incorporation is consistent with increased bond strengths of the bridging V-O-V groups in the composite. This cannot be attributed to increased V^{4+} content in the materials as a result of reaction with the pyrrole monomer. Although the electrochemistry results (*vide infra*) confirm the increasing formation of V^{4+} with increasing polymer content, it is evident that another effect dominates the shifts in the IR bands. One tentative mechanism that may account for the observed increase in V-O-V bonding interaction is based on the change in coordination geometry at the metal center. The vanadium ions in V_2O_5 adopt a square pyramidal coordination with the V atoms occupying a position slightly above the basal plane.[20] The distorted geometry is facilitated by the strong V=O interaction. A decrease in V=O interaction in the nanocomposite material is likely to alter the coordination geometry. A change in position of the V ion, caused by decreased axial interaction, such that it occupies a position in the VO_4 plane will result in increased in-plane bonding interactions. The V-O-V groups in the V_2O_5-based materials lie in the plane and the strong H-bonding induced elongation of V=O bond is likely to induce structural distortions at the metal center that can account for the observed strengthening of the V-O-V bonds.

Influence of the Interaction

The experimental results indicate that the interaction influences at least three different physical properties; the microstructure, the electrical conductivity and the electrochemical response.

We chose a simultaneous polymerisation method for the formation of the nanocomposites, as prior work has shown that it leads to optimum mixing at the molecular level, and hence a homogeneous matrix. In this system, polymerisation to form the PPy network is effectively caused by a redox reaction with the inorganic component, leading to the formation of V^{4+} which in turn catalyzes the rate of the condensation of the V_2O_5 network. The latter effect is well-known for the corresponding V_2O_5 xerogels.[2,21] It is demonstrated here by the considerably shorter gelation time for the system. Thus we have a "double" polymerisation process that results in a homogenous composite as desired, but one in which the rapid polymerisation rate of the inorganic polymer leads to interrupted growth of the characteristic ribbon morphology of V_2O_5, as shown in the TEM photomicrographs.

The microstructure of the organic/inorganic nanocomposite has a profound effect on the electrical conductivity. In the case of simultaneous polymerisation, the truncation of this fibrous structure by interaction with the occluded PPy disrupts charge transport within the continuous V_2O_5 phase. We see a direct correlation of lower conductivity with increased PPy content, and shift of the ν_{sym} V-O-V band. Conversely, the dispersion method leads to isolated PPy particles encapsulated in the continuous V_2O_5 phase. In this case, the addition of PPy has no effect on the gelation rate of the V_2O_5, enabling the characteristic V_2O_5 ribbon structure to develop. Thus, the observed conductivities are independent of PPy content and comparable to that of the pristine V_2O_5 ARG. The expected conductivity increase upon addition of the conductive polymer was not observed because the particles were effectively isolated and did not form a continuous phase within the matrix.

A third influence of the PPy-V_2O_5 interaction is that on the electrochemical Li insertion properties. The formation of PPy leads to the creation of V^{4+} centers, and therefore decreases the Li capacity. In principle, two electrons are lost from the V_2O_5 in the coupling of each monomer unit in the polymerisation step:

$$y\ (\text{pyrrole}) + V_2O_5 \Rightarrow [\text{poly(pyrrole)}]_yV_2O_{5-2y} \leftrightarrow [PPy^{z+}]_y[V_2O_{5-2y}]^{z-}$$

Although the second oxidation step (doping) represents a reversible redox process from a thermodynamic point of view, the first step does not. The linear variation of the first discharge capacity with PPy content (**Figure 8**) reflects this. Note that the observed capacity decreases are what one would predict from

consideration of the polymer ratio and the two electron reduction process above, starting from a partially reduced V_2O_5 lattice (~ 10% V^{4+}), in combination with some reoxidation of the V centers by exposure to air.[6b]

As these materials possess a mixed valence V^{5+}/V^{4+} state counterbalanced by the presence of mobile species (protons) and oxidizable polymer, it was of interest to investigate the effect of subjecting the electrode to a initial oxidation (charge process). During this process, oxidation of redox centers from V^{4+} to V^{5+} can occur, along with possible additional doping of the polymer involving further oxidation. In either case, electrochemical oxidation would be accompanied by expulsion of H^+ or insertion of ClO_4^- anions. No well-defined oxidation peak was observed for an initial charge up to 3.8V, although a gain in total reversible capacity was observed. For nanocomposites with a small PPy content $0< \mathbf{P} <0.6$, the capacity increase during the charge process is almost what one would expect from reoxidation of the reduced components. For example, the capacity of $[PPy]_{0.3}V_2O_5$ increases from 1.6F/mol to 1.85F/mol during charge.

At higher PPy ratios (where $\mathbf{P} >0.6$), the gain in capacity is less than expected, and dependent on whether the oxidation precedes or follows the discharge process. This behavior has been previously observed in the electrochemical response of polymer/V_2O_5 xerogels (polymer = polythiophene and polypyrrole) and was attributed to restricted access of Li^+ owing to blockage by excessive surface polymer.[8b,c]

Chemical oxidation can be used to even greater benefit, to regain the lost capacity in these materials, similar to that observed previously for polymer/V_2O_5 xerogels.[8a,b] In particular, the post-oxidative treatment drastically improves the electrochemical response *via* direct effect on the redox centers, and gives rise to increased capacity for O_2-$[PPy]_{0.3}V_2O_5$ (2.2F/mol to a discharge voltage of 1.8V). At a wider voltage window of 3.8-1.2V (**Figure 12**), the capacity of the pristine V_2O_5 ARG is 2.7F/mol, and is increased to 3.8F/mol for the O_2-treated $[PPy]_{0.3}V_2O_5$ nanocomposite.

A more detailed comparison of the electrochemical behaviour of this system with the that of the "microcomposite" PPy-V_2O_5 will be reported in a subsequent paper.[22]

Conclusions

Polypyrrole/vanadium pentoxide aerogel maerials were synthesized by two different sol-gel routes with the simultaneous polymerisation method being investigated in greater detail. The resulting organic/inorganic materials are typical of ARGs in that they possess low density (0.1 to 0.2 g/cc) and high surface area (150-250 m^2/g). The materials are characterized by strong interactions between the organic and inorganic components which influence the electrical and electrochemical properties of the nanocomposite. This interaction is evident by shifts in the V=O and V-O-V modes and is attributed to strong H-bonding interactions and alteration of the coordination geometry, respectively. This interaction and changes in the aerogel microstructure lead to progressively lower electrical conductivity upon addition of PPy to the nanocomposite. Since the formation of PPy leads to creation of V^{4+} centres, lithium capacity decreases with PPy content. This lost capacity is regained by oxidation treatments, however. The electrochemical results demonstrate the ability of PPy/V_2O_5 aerogel nanocomposites to exhibit a substantial improvement in lithium capacity as compared to the pristine oxide.

Acknowledgements

The financial support of this research by the Office of Naval Research (BD) and the Natural Sciences and Engineering Councial of Canada (LFN) is gratefully acknowleged.

List of Figure Captions

Figure 1. Compositions of nanocomposites synthesized with a pyrrole ratio of 0.15. The arrows represent the relative mechanical integrity of the gels.

Figure 2. TGA curve for the $[PPy]_{0.5}V_2O_5$ nanocomposite aerogel, heated at 10°C/min in air.

Figure 3. TEM micrographs of a) V_2O_5 aerogel; and b) $[PPy]_{0.5}V_2O_5$ nanocomposite aerogel prepared by simultaneous polymerisation, showing the interrupted chain growth; c) SEM micrograph of $[PPy]_{1.0}V_2O_5$ microcomposite prepared by the dispersion method.

Figure 4. FTIR spectra comparing V_2O_5 (^{18}O-labelled) and V_2O_5/PPy composite aerogels showing effects of PPy incorporation on ν_{sym}(V-O-V), ν_{as}(V-O-V) and ν(V=O).

Figure 5. FTIR spectra of the V=O bond showing the effects of D_2O labelling; a) V_2O_5 aerogel; b) V_2O_5/PPy composite aerogel.

Figure 6. Conductivity - temperature plot of of $PPy_{2P}V_2O_5$ aerogels where P= 0 - 1. The + data points are for pure V_2O_5 (P=0). b) Conductivity - temperature plot of PPy/V_2O_5 aerogels prepared by the dispersion method.

Figure 7. a) Modification of the electronic density *vs* voltage curves as a function of the discharge cut-off (1.8 and 1.2V) for V_2O_5-ARG at 10μA/cm^2; cycles are indicated on the plot; b) cyclic voltamogramms of V_2O_5-ARG corresponding to a 10mV/0.2h voltage step; and a 10mV/0.02h voltage step, in the voltage window between 1.4-4.0V.

Figure 8. Evolution of the first discharge curves as function of the polymer content (2P), in $[PPy]_yV_2O_5$ at 10μA/cm^2.

Figure 9. Evolution of the electronic density *vs* voltage cuves as function of the polymer content in the nanocomposites. The curves were obtained by numerical differentiation of the plots shown in Figure 8.

Figure 10. Effect of the oxidative treatment on $[PPy]_{0.3}V_2O_5$; discharge-charge curves are shown for materials prepared using an *in-situ* oxidative treatment with a molar ratio $(NH_4)_2S_2O_8$/

V_2O_5 of 0.1, 0.2 and 0.3. The fourth curve shows $[PPy]_{0.3}V_2O_5$ after O_2 treatment for comparison. A cycling rate corresponding to the intercalation of 1.0 Li in 20hr (C/20) was used.

Figure 11. Illustration showing proposed interaction of the PPy with the V_2O_5 framework.

Figure 12. Voltage *vs* composition curves for a) the post-oxidation for aerogel electrodes in the 3.8-1.2V window, at a constant current of 10 $\mu A/cm^2$. (1) V_2O_5 aerogel; (2) the post-oxidized nanocomposite aerogel O_2-$[PPy]_{0.3}V_2O_5$.

List of Tables

Table 1. Comparison of physical and electrical properties for $[Ppy]_{2P}V_2O_5$ aerogels.

Composition	$[Ppy]_{2P}V_2O_5$ P	ρ (g/cc)	σ T=25°C (S/cm)	Surface Area (m^2/g)	Oxidizing agent added
V_2O_5	0	0.10	$2x10^{-4}$	150	No
$[Ppy]_{0.6}V_2O_5$	0.3	0.19	$2x10^{-4}$	184	No
$[Ppy]_{0.6}V_2O_5$	0.3	-	-	257	Yes
$[Ppy]_{1.0}V_2O_5$	0.5	0.22	$2x10^{-6}$	-	No
$[Ppy]_{1.4}V_2O_5$	0.7	0.20	$4x10^{-7}$	179	No
$[Ppy]_{1.8}V_2O_5$	0.9	0.25	$2x10^{-8}$	-	No
$[Ppy]_{2.0}V_2O_5$	1.0	0.15	-	160	No
$[Ppy]_{2.0}V_2O_5$	1.0	0.12	$2x10^{-6}$	200	Yes
microcomposite $[Ppy]_{1.0}V_2O_5$	0.5	0.14	$3x10^{-4}$		pre-polymerized
microcomposite $[Ppy]_{2.0}V_2O_5$	1.0	0.18	$3x10^{-4}$	140	pre-polymerized
microcomposite $[Ppy]_{3.0}V_2O_5$	1.5	0.16	$3x10^{-4}$		pre-polymerized
microcomposite $[Ppy]_{6.0}V_2O_5$	2.0	0.19	$3x10^{-4}$	80	pre-polymerized

Table 2. Effects of PPy intercalation upon ν_{sym}(V-O-V)

Sample	*frequency (cm^{-1}) of ν_{sym}(V-O-V)*
V_2O_5	542
$[Ppy]_{0.4}V_2O_5$	565
$[Ppy]_{0.5}V_2O_5$	574
$[Ppy]_{1.0}V_2O_5$	580

References

1. F. Chaput, B. Dunn, P. Fuqua, and K. Salloux, *J. Non-Cryst. Solids*, 1995, **188**, 11.
2. J. Livage, *Chem. Mater.*, 1991, **3**, 578.
3. B. Katz, W. Liu, K. Salloux, F. Chaput, B. Dunn, and G.C. Farrington, *Mat. Res. Soc. Symp. Proc.*, 1995, **369,** 211; D.B. Le, S. Passerini, A.L. Tipton, B.B. Owens, and W.H. Smyrl, *J. Electrochem. Soc.*, 1995, **142,** L102; D.B. Le, S. Passerini, J. Guo, J. Ressler, B.B. Owens and W. H. Smyrl, *J. Electrochem. Soc.*, 1996, **143**, 2101.
4. B. Scrosati, in *Solid State Electrochemistry.*,1995, ed. P.G. Bruce, p 229, Cambridge University Press, Inc., Cambridge, Great Britain and refs therein.
5. S. Panero, E. Spila, B. Scrosati, *J. Electrochem. Soc.*, 1996, **143**, L29; K. Naoi, M. Lien, and W.H. Smyrl, *J. Electrochem. Soc.*, 1991, **138**, 440.
6. M. Kanatzidis, C-G Wu, H.O. Marcy, and C.R. Kannewurf, *J. Am. Chem. Soc.*, 1989, **111**, 4139; C-G. Wu, D.C. DeGroot, H.O. Marcy, J.L. Schindler, C.R. Kannewurf, Y.J.-Liu, W. Hirpo and M. Kanatzidis, *Chem. Mater.*, 1996, **8**, 1992.
7. C-G. Wu, M. Kanatizidis, H.O. Marcy, and C.R. Kannewurf, *Polym. Mater. Sci. Eng*, 1989, **61**, 969.
8. F. Leroux, B. E. Koene, and L.F. Nazar, *J. Electrochem. Soc.*, 1996, **143**, L181-182; F. Leroux, G.R. Goward, and L.F. Nazar, *J. Electrochem. Soc.*, 1997, **144**, 3886-3895; G.R. Goward, F. Leroux and L.F. Nazar, *Electrochimica Acta*, in press.
9. B.E. Koene, and L.F. Nazar, *Solid State Ionics,* 1996, **89**, 147-157.
10. T.A. Kerr, H. Wu, L.F. Nazar, *Chem. Mater.*, 1996, **8**, 2005; L.F. Nazar, H. Wu, and W.P. Power, *J. Mater. Chem.*, 1995, **5**, 1985.
11. B.C. Dave, B. Dunn, F. Leroux, L.F. Nazar, and H.P. Wong, *Mat. Res. Soc. Symp Proc., Better Ceramics Through Chemistry VII*, 1996, **435**, 611.
12. S. Maeda and S.P. Armes, *J. Colloid Interface Sci.* 1993, **159**, 257; S. Maeda and S.P. Armes, *J. Mater. Chem.* 1994, **4**, 935; S. Kuwabata, A. Kishimoto, T. Tanaka, H. Yoneyama, *J. Electrochem. Soc.*, 1994, **141**, 10; A.H. Gemeay, H. Nishiyama, S. Kuwabata, H. Yoneyama, *J. Electrochem Soc*, 1995, **142**, 4190.
13. W.A. Wampler, K. Rajeshwar, R.G. Pethe, R.C. Hyer and S. C. Sharma, *J. Mater. Res.* 1995, **10**, 1811.
14. R.E. Myers, *J. Electronic. Mater.*, 1986, **15**, 61.
15. J. Lei, Z. Cai and C. R. Martin, *Synth. Met.*, 1992, **46**, 53; J. Lei, Z. Cai and C. R. Martin, *ibid.*, 1992, **48**, 301.
16. M. R. Bond, R. S. Czernuszewicz, B. C. Dave, Q. Yan, M. Mohan, R. Verastegue, C. Carrano, *Inorg. Chem.*,1995, **34**, 5857.
17. J.-M. Savariault, D. Lafargue, J.-L. Parise, and J. Galy, *J. Solid State Chem.* 1992, **97**, 169.
18. Y.-J. Liu, D. C. DeGroot, J. L. Schindler, C. R. Kannewurf, and M. G Kanatzidis, *J. Chem. Soc. Chem. Commun*, 1993, 593.
19. E. Ruiz-Hitzky, and B. Casal, *J. Chem. Soc. Faraday Trans.*, 1986, **82**, 1597.
20. T. Yao, Y., Oka, and N. Yamamoto, *Mat. Res. Bull.* 1992, **27**, 669; P. Aldebert, N. Baffier, N. Gharbi, and J. Livage, *Mat. Res. Bull.* 1981, **16**, 669.
21. J. Lemerle, L. Nejem, and J. Lefebvre, *J. Chem Res.*, 5301 (1978).
22. B. Dunn, J. Herreld, F. Leroux, L.F. Nazar and K. Salloux, manuscript in preparation.

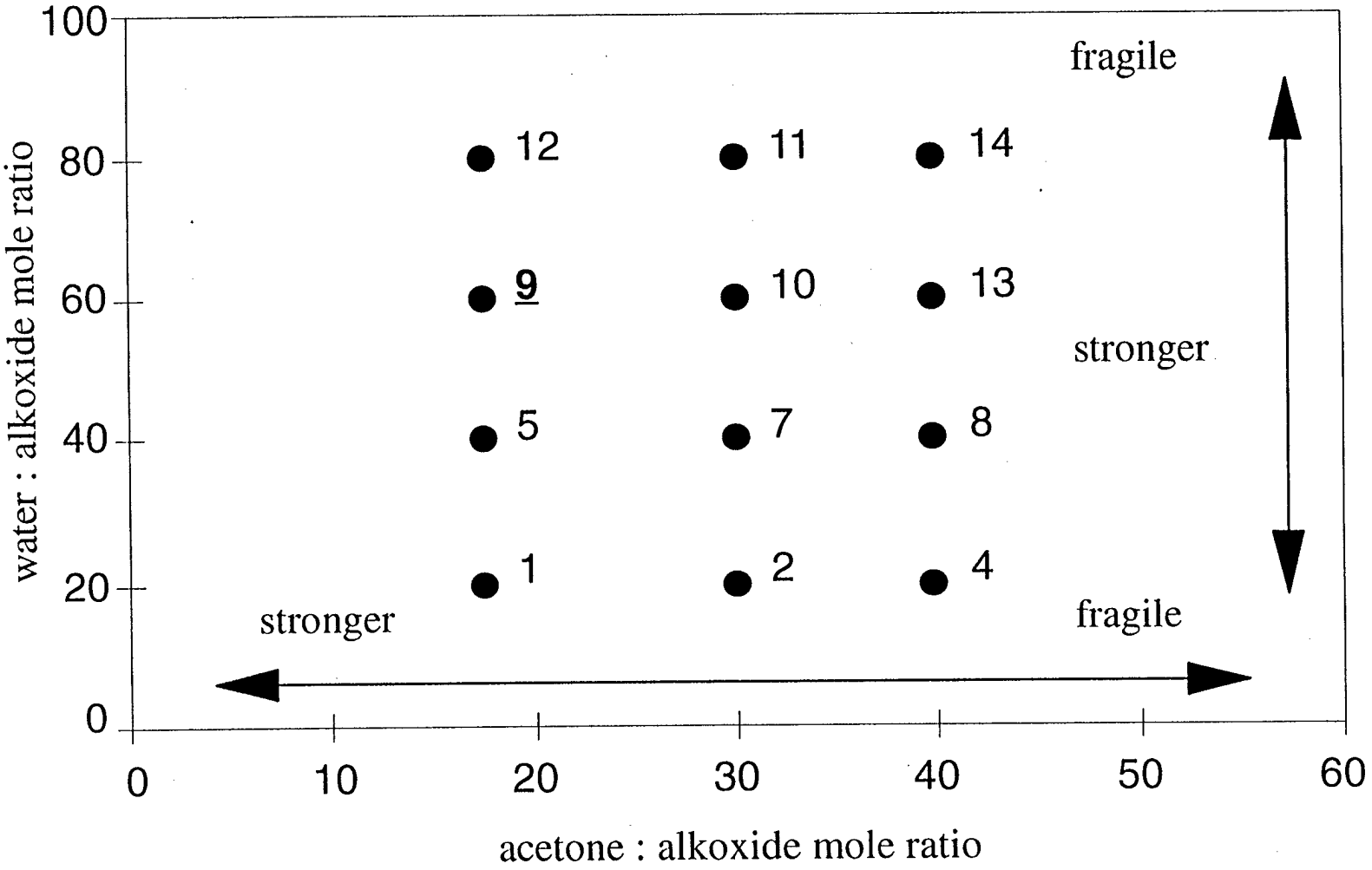
100
80
60
40
20
0
water : alkoxide mole ratio
0
10
20
30
40
50
60
acetone : alkoxide mole ratio
12
11
14
9
10
13
5
7
8
1
2
4
fragile
stronger
stronger
fragile

figure 1

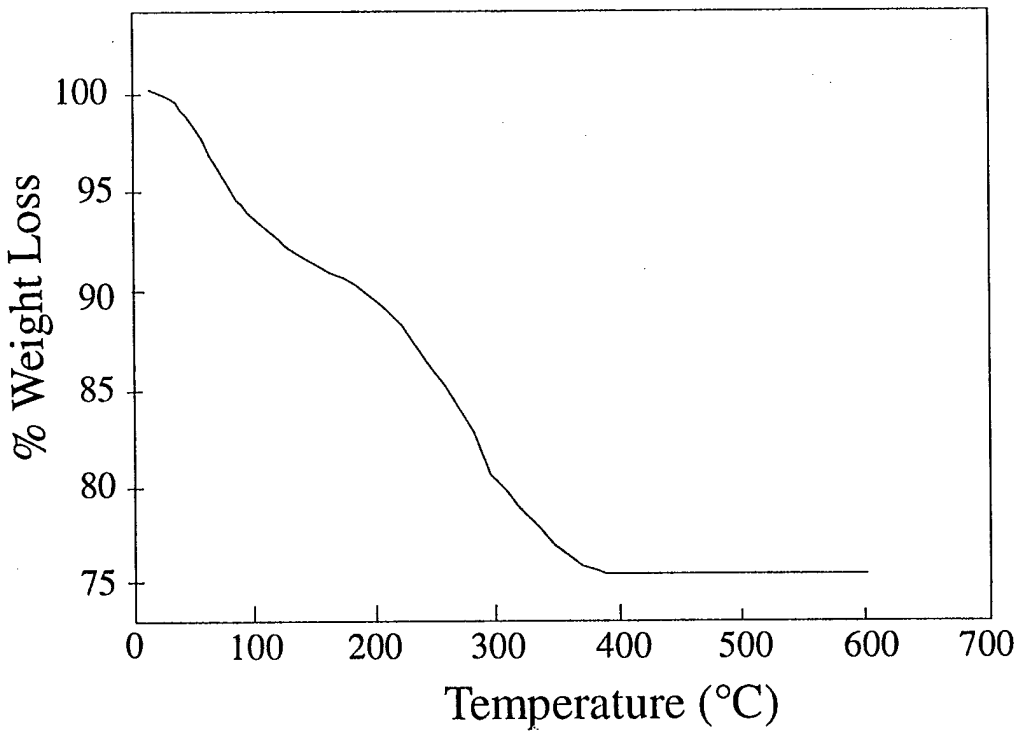
% Weight Loss
100
95
90
85
80
75
0
100
200
300
400
500
600
700
Temperature (°C)

figure 2

a)

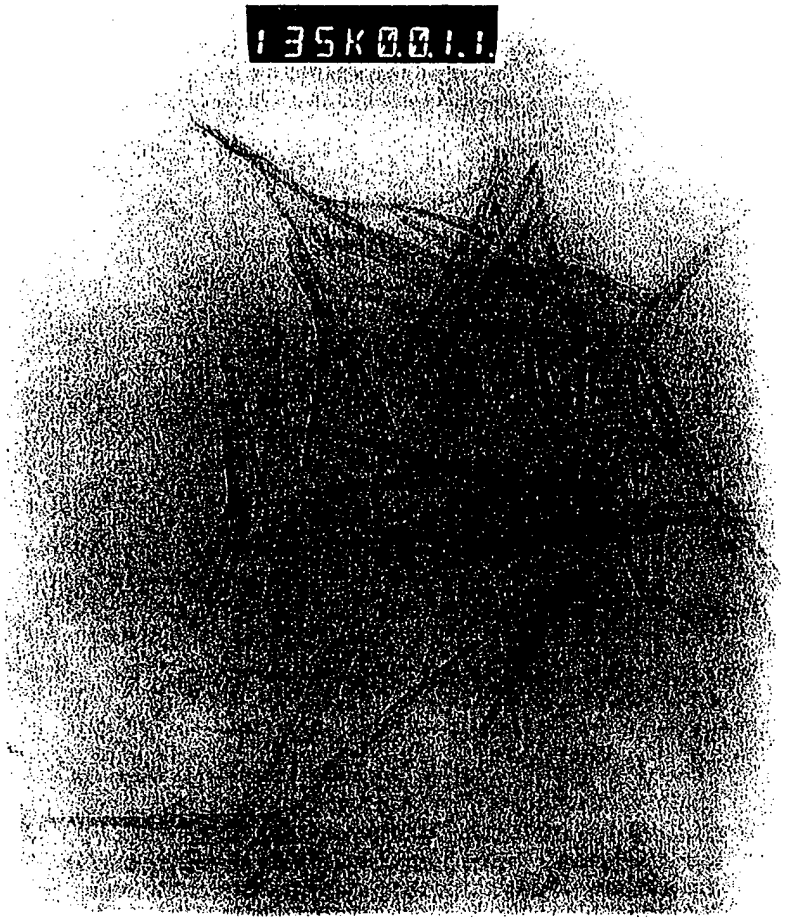

b)

figure 3

c)

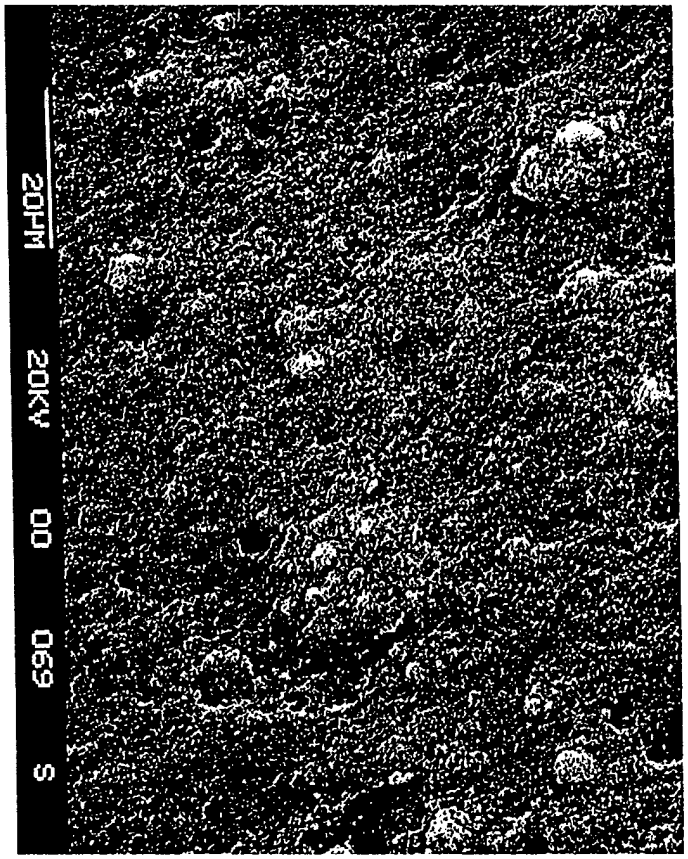

figure 3c

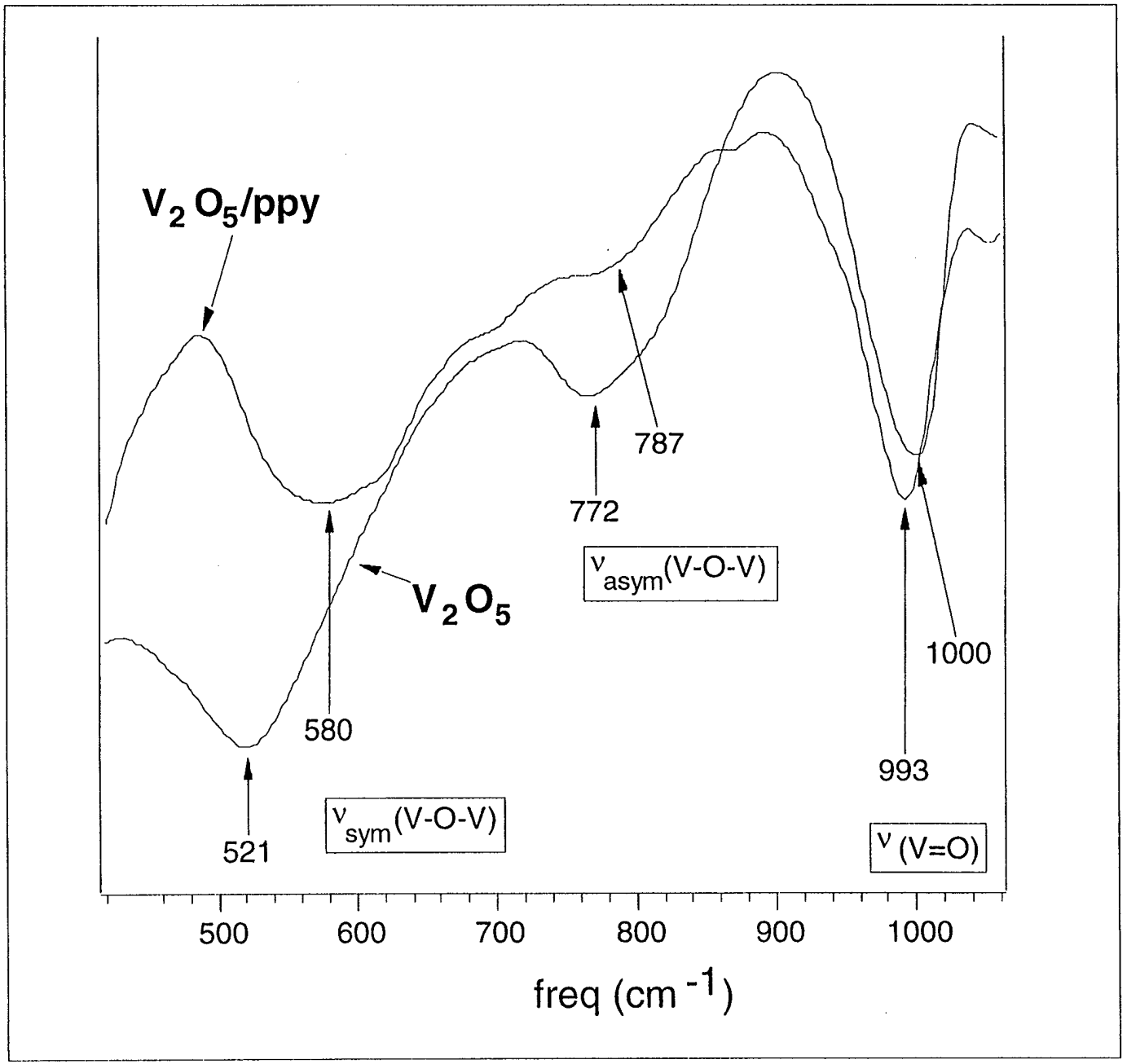
V2 O5/ppy
787
772
νasym(V-O-V)
V2O5
1000
580
993
521
νsym(V-O-V)
ν (V=O)
500
600
700
800
900
1000
freq (cm -1)

figure 4

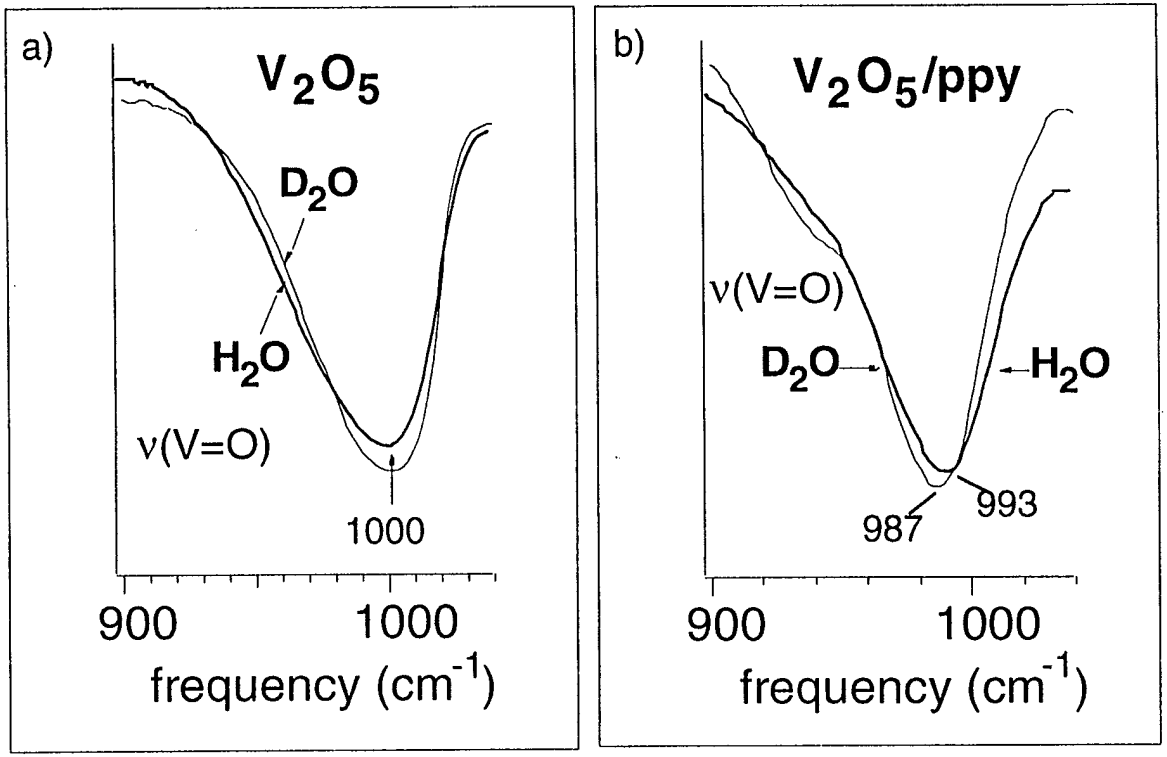
a)
V_2O_5
D_2O
H_2O
ν(V=O)
1000
900
1000
frequency (cm^{-1})
b)
V_2O_5/ppy
ν(V=O)
D_2O
H_2O
987
993
900
1000
frequency (cm^{-1})

figure 5

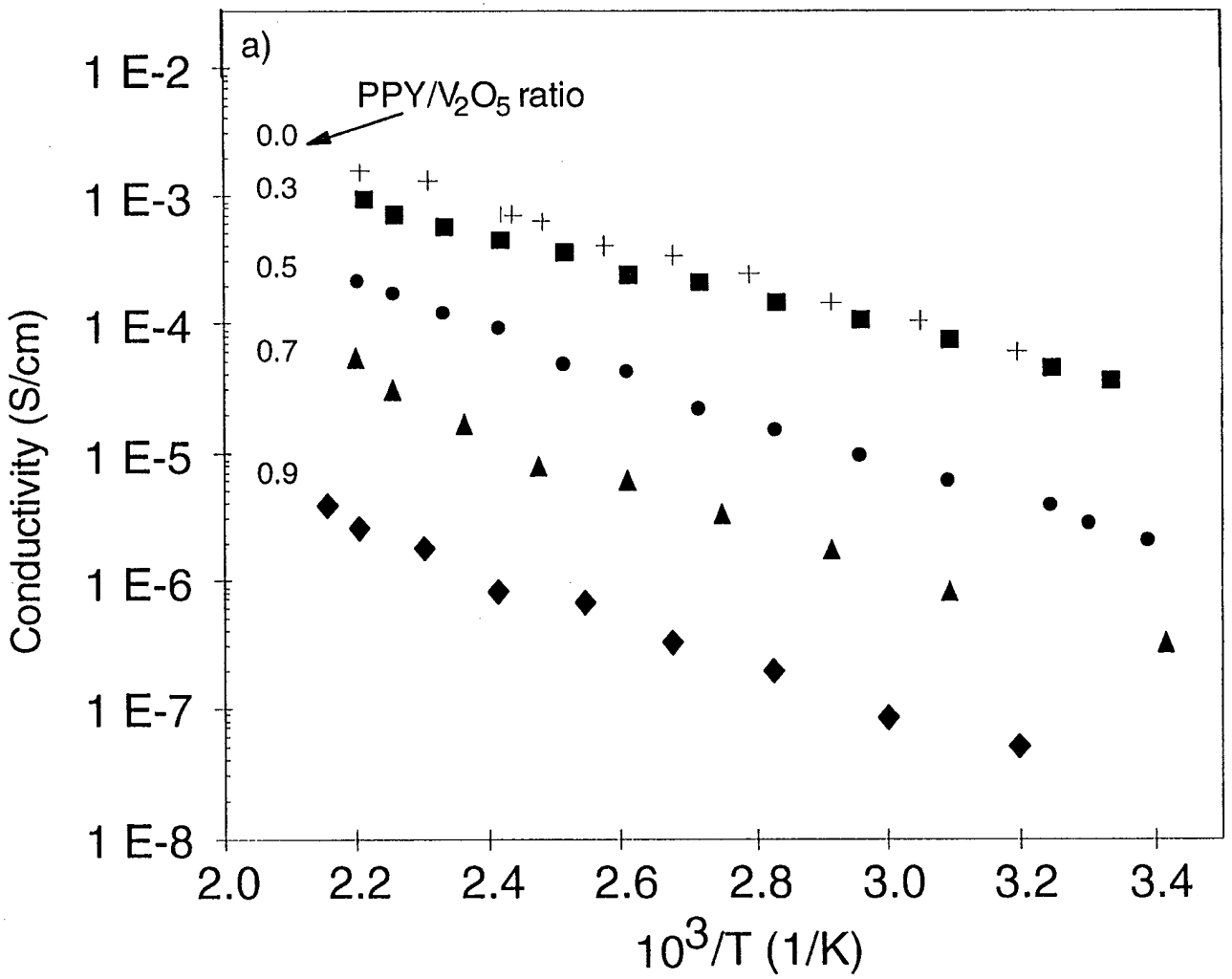
a)
PPY/V2O5 ratio
0.0
0.3
0.5
0.7
0.9
Conductivity (S/cm)
1 E-2
1 E-3
1 E-4
1 E-5
1 E-6
1 E-7
1 E-8
2.0
2.2
2.4
2.6
2.8
3.0
3.2
3.4
10^3/T (1/K)

figure 6a

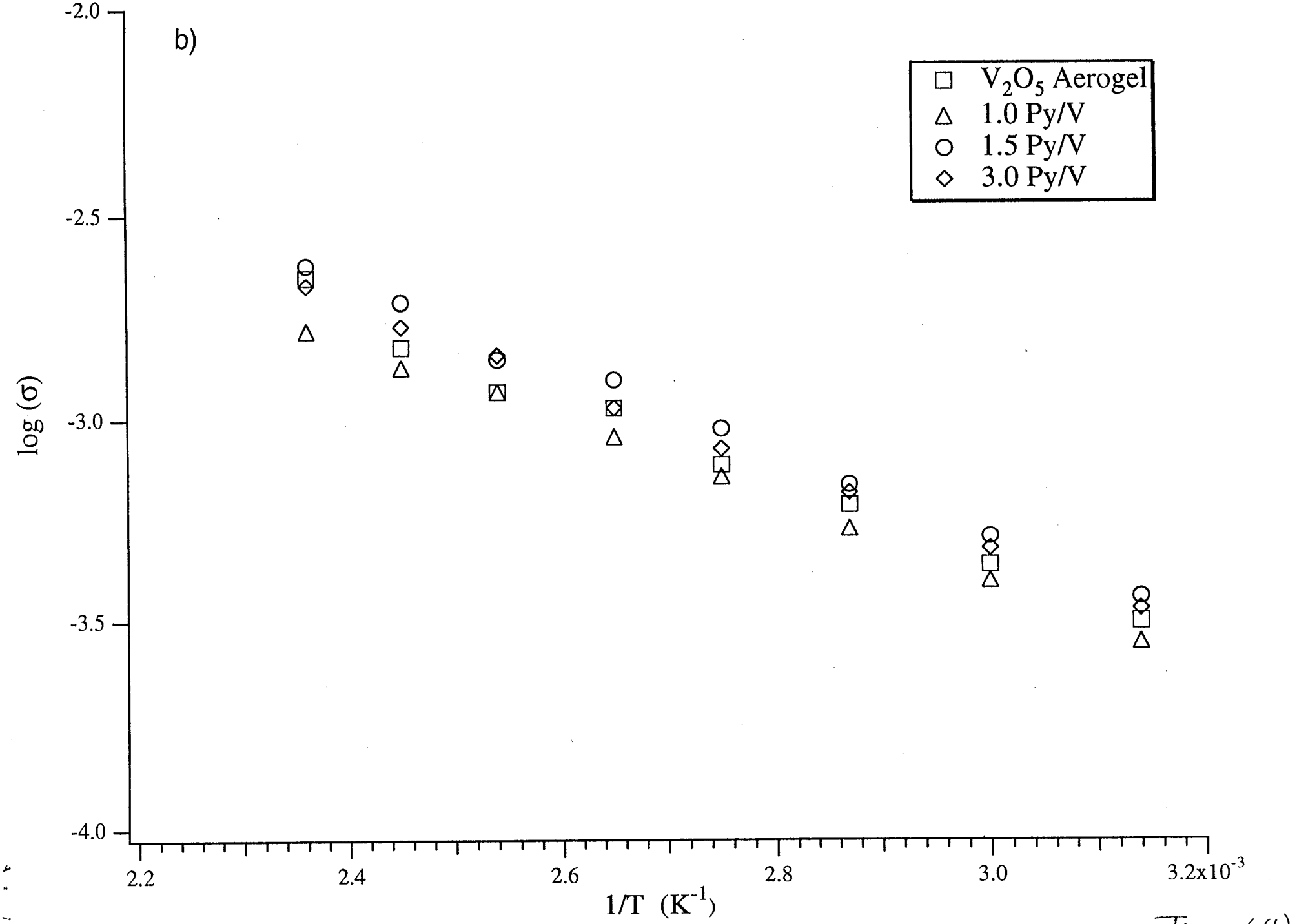
b)
V_2O_5 Aerogel
1.0 Py/V
1.5 Py/V
3.0 Py/V
log (σ)
-2.0
-2.5
-3.0
-3.5
-4.0
2.2
2.4
2.6
2.8
3.0
3.2x10^{-3}
1/T (K^{-1})

Figure 6(b)

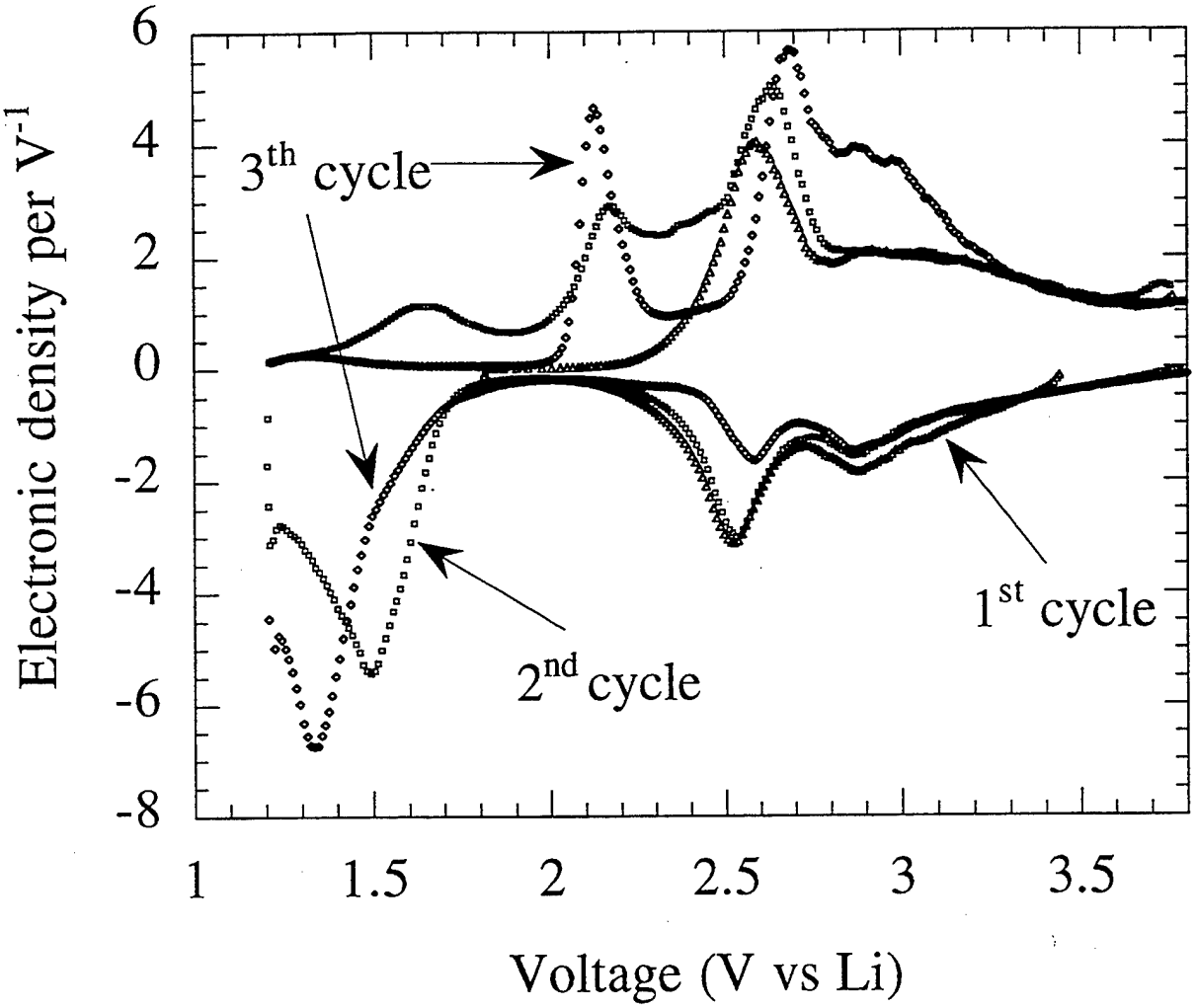
6
4
2
0
-2
-4
-6
-8
1
1.5
2
2.5
3
3.5
Electronic density per V-1
Voltage (V vs Li)
3th cycle
2nd cycle
1st cycle

Figure 7a

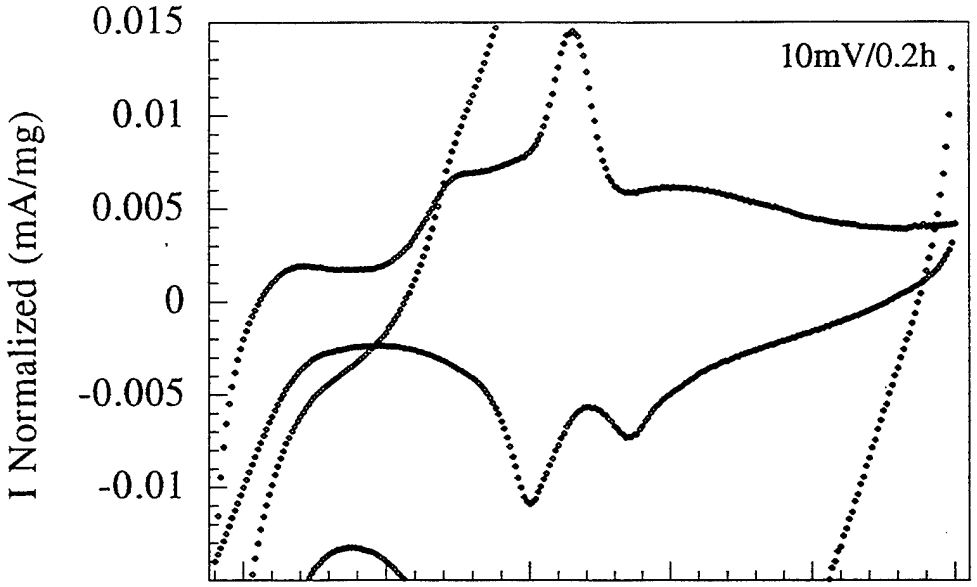

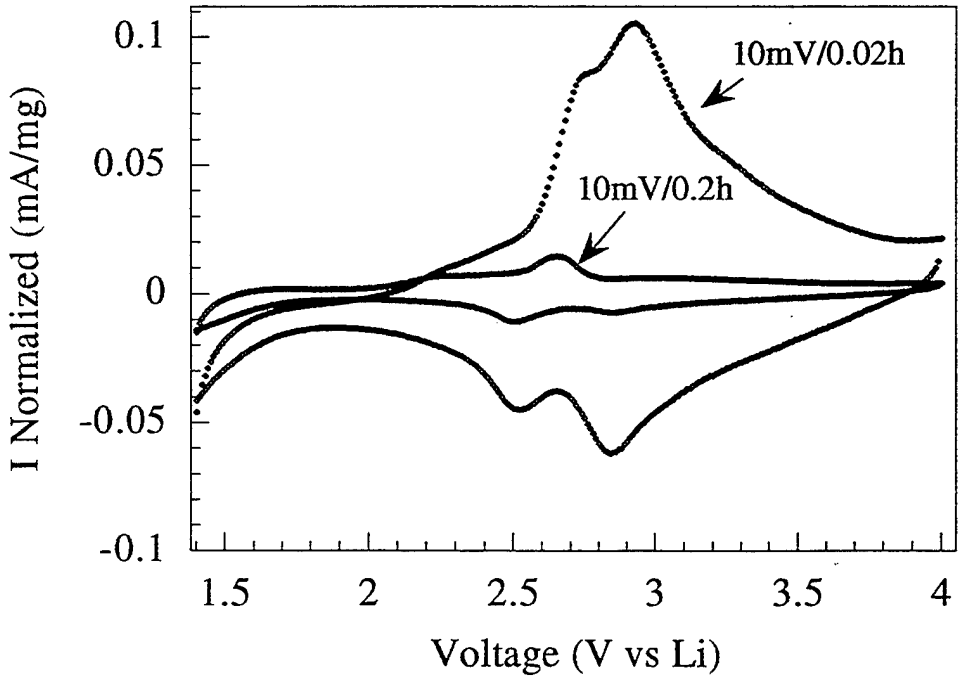

Figure 7b (revised)

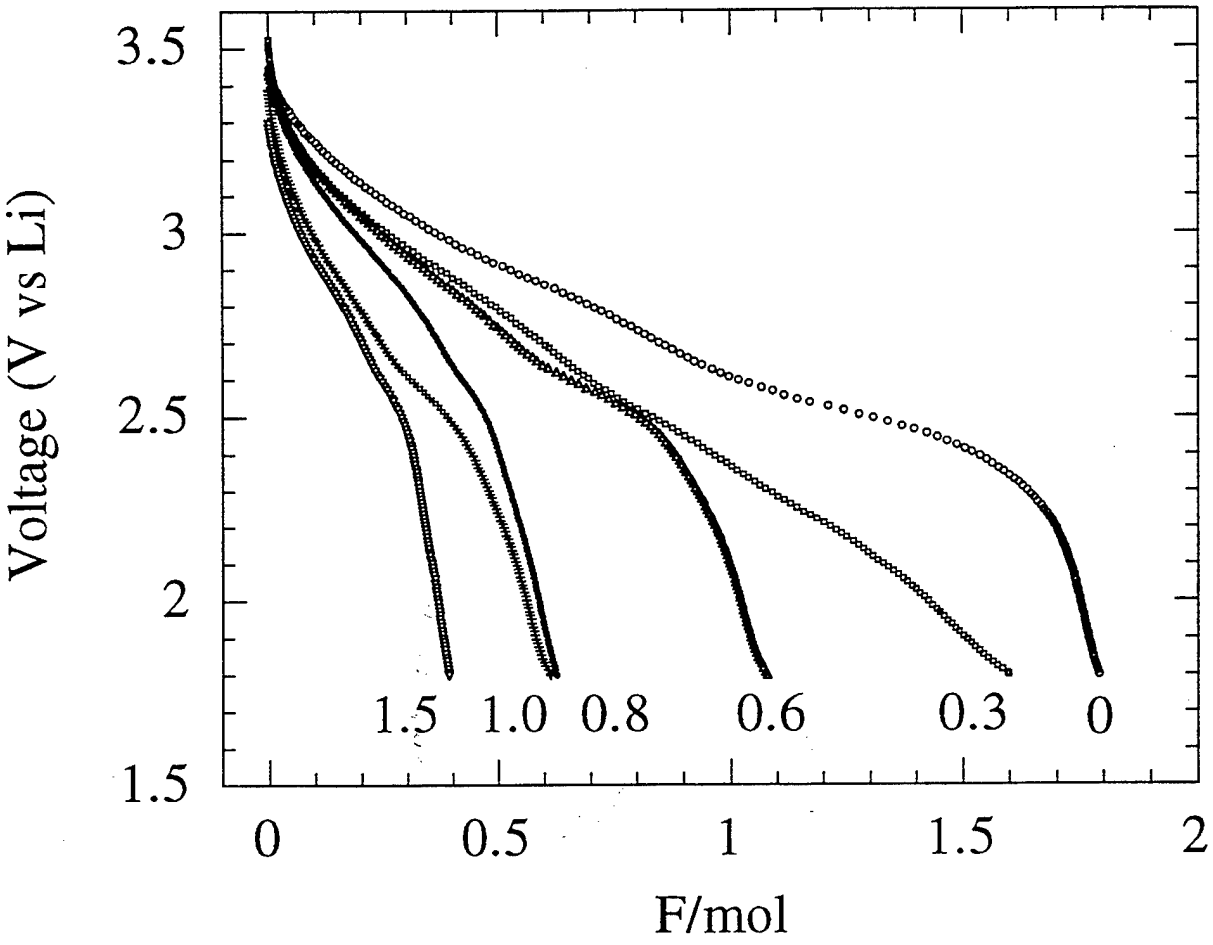

Figure 8

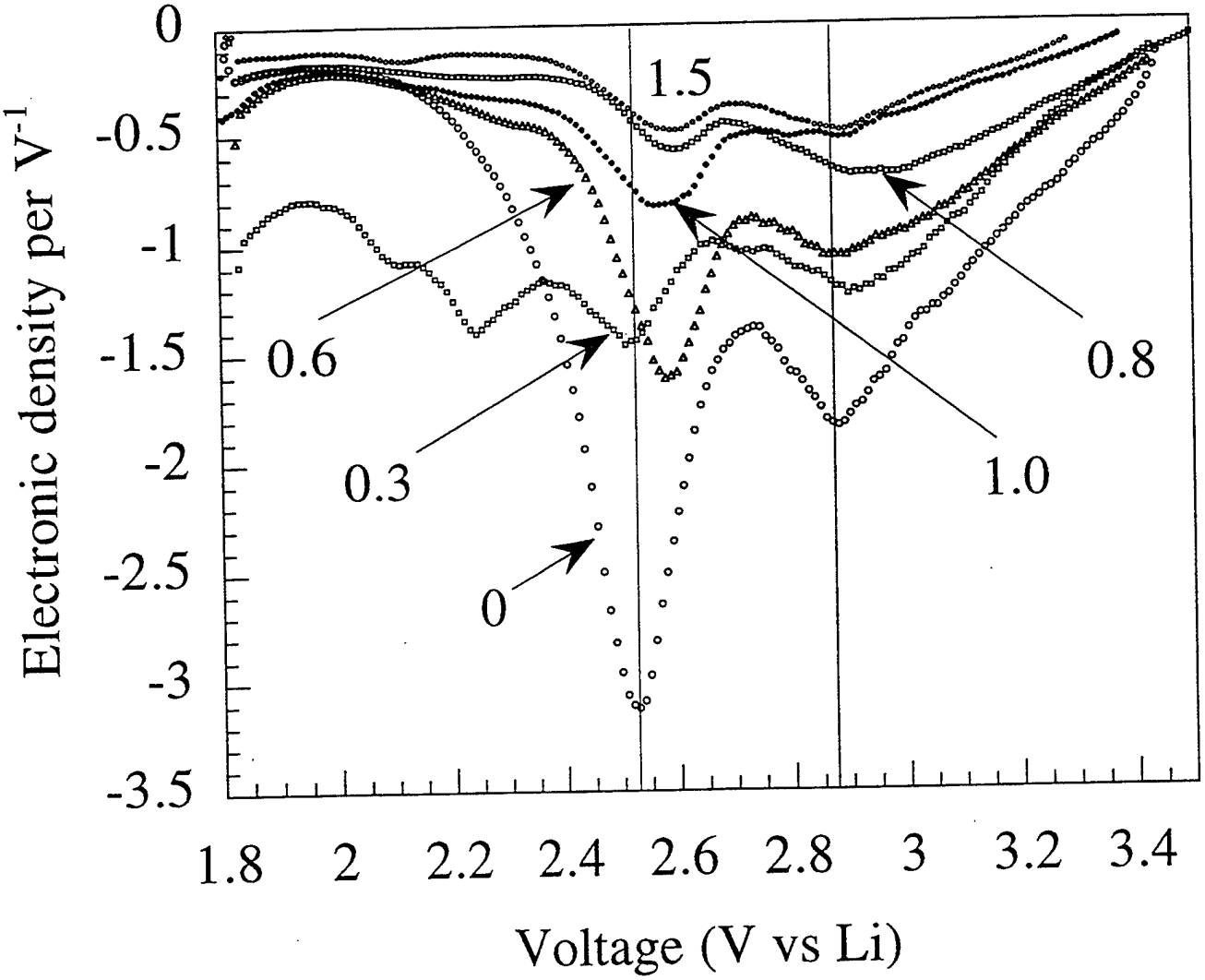
0
-0.5
-1
-1.5
-2
-2.5
-3
-3.5
Electronic density per V-1
1.5
0.6
0.8
0.3
1.0
0
1.8
2
2.2
2.4
2.6
2.8
3
3.2
3.4
Voltage (V vs Li)

Figure 9

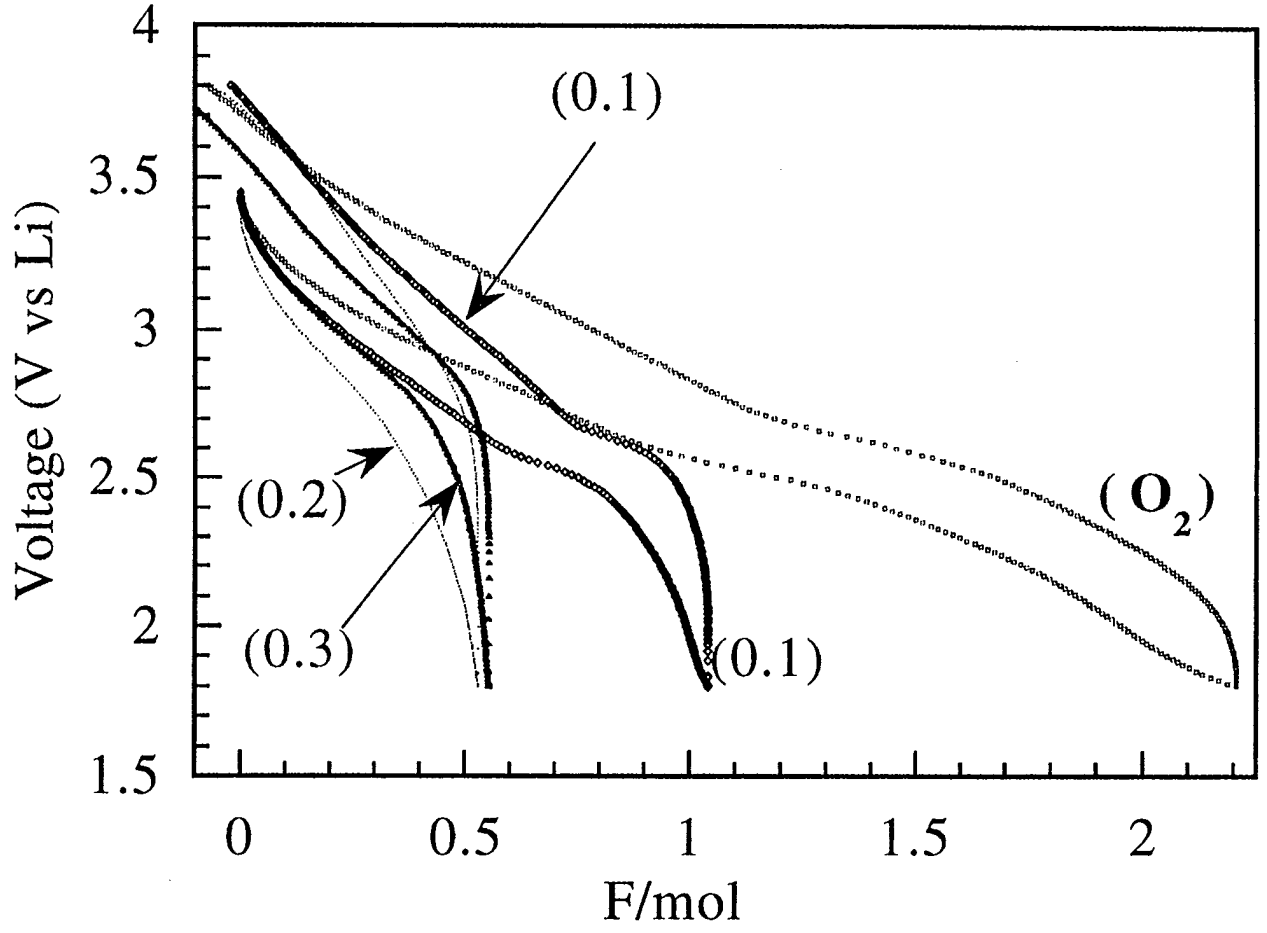

Figure 10
(revised)

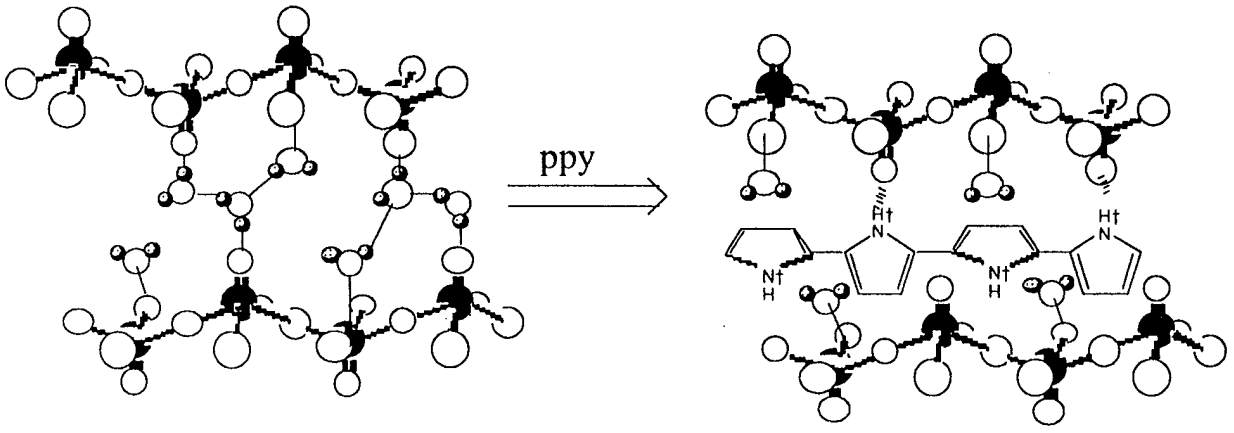

V_2O_5 V_2O_5.ppy

Figure 11 or Scheme 1

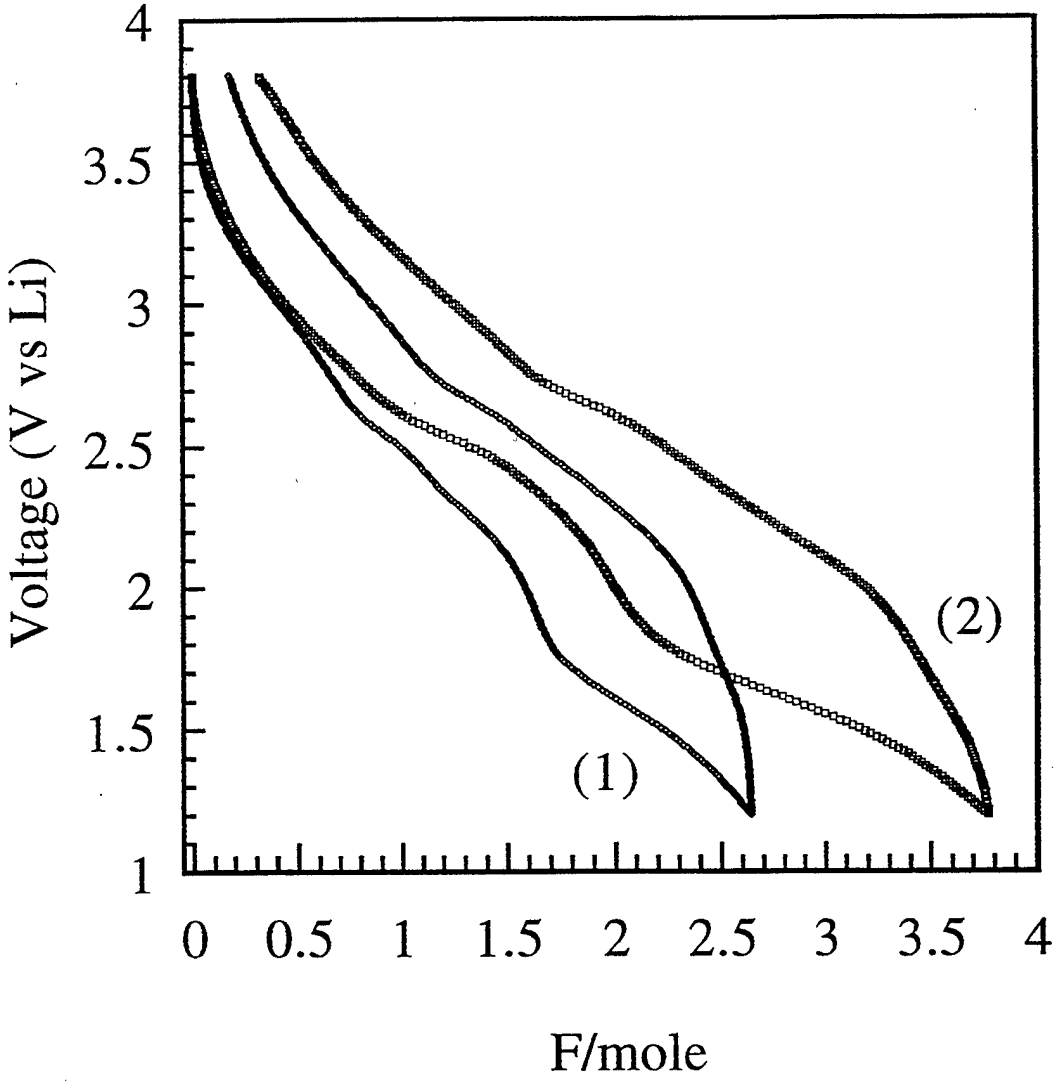

Figure 12